INTERNATIONAL JOURNAL FOR NUMERICAL METHODS IN FLUIDS
Int. J. Numer. Meth. Fluids 2003; **41**:789–808 (DOI: 10.1002/fld.418)

The use of dynamic grid adaptation algorithms for the modelling of flow around a circular cylinder in sub-critical flow regime

G. de With[1], A. E. Holdø[1,*,†] and T. A. Huld[2]

[1] *CFD Research Group, Department of Aeronautical, Civil and Mechanical Engineering, University of Hertfordshire, Hatfield, U.K.*
[2] *Institute for Systems, Informatics and Safety, Joint Research Centre, Ispra (Va), 21020, Italy*

SUMMARY

In the present study a dynamic grid adaptation (DGA) algorithm is utilized for predicting flow around a circular cylinder in sub-critical flow regime at a Reynolds number of 1.4×10^5. The reason for adopting a DGA algorithm is the unsteadiness of the flow field which makes a conventional mesh inefficient. The concept being adopted is to concentrate mesh refinement in regions with high gradients and high turbulent viscosity, while in the region further downstream where the flow is fully developed a coarser mesh will develop and turbulence is modelled with the large eddy simulation (LES) turbulence model.

The aim of the study is to present an appropriate variable for mesh refinement, which accomplishes a high rate of mesh refinement in the region with high gradients. The new variable is a product of the local mesh cell size and the rate of strain and includes two additional variables to allow control over the refinement behaviour. The results are compared with experimental data at the corresponding Reynolds number and also with numerical results obtained with conventional mesh. It is demonstrated that DGA algorithms can give results of a very high quality for a mesh that is significantly smaller than for a conventional mesh. Copyright © 2003 John Wiley & Sons, Ltd.

1. INTRODUCTION

The present study deals with the simulation of flow around a circular cylinder at a Reynolds number of 1.4×10^5. Several studies have been reported for this type of flow [1] and it is gradually accepted that it is a difficult test case for computational fluid dynamics (CFD) [2]. Tutar and Holdø's results suggest that the large eddy simulation (LES) method gives improved results compared to those of other Reynolds averaging Navier Stokes (RANS) based turbulence models and Breuer [2] demonstrates the considerable mesh requirements of the LES type of simulations. In order to overcome the mesh requirements and still obtain results of good quality the present work investigates the suitability of a dynamic grid adaptation (DGA) algorithm.

* Correspondence to: A. E. Holdo, Department of Aerospace, Aeronautical, Civil & Mechanical Engineering, University of Hertfordshire, Hatfield, Herts AL10 9AB, U.K.
† E-mail: a.e.holdo@herts.ac.uk

Received August 2001
Revised 24 June 2002

Frequently meshes are generated where due to mesh construction methods the resolution is high in regions where gradients are not significant. Consequently, such meshes have a large number of redundant cells. Conversely, due to time variations in the computed flow field, there will be regions where the mesh resolution is insufficient. The aim of the present work was to use DGA methods to generate mesh refinement in important regions and conversely to reduce mesh refinement in regions with low gradients.

To achieve this aim it was necessary to define and develop mesh refinement variables. There have been many developments related to adaptive methods and adaptive grid strategies [3–6]. However, there is comparatively little work reported on grid adaptation with turbulent, unsteady flows. The present work is focussed on the determination of a reliable refinement variable.

In this work the CFD code REACFLOW [7] has been utilized. This code has adopted the projection method in the solution procedure and uses a triangular mesh. Due to the triangular mesh being used in the REACFLOW code the definition of the length scale in the LES turbulence model has to be considered. The LES turbulence model belongs to the Eddy viscosity type of turbulence models and calculates the turbulent viscosity element wise from both the rate of strain and the cell size of the element. In this work two methods for calculating the length scale are presented.

2. BACKGROUND

The work being undertaken focusses both on grid adaptation and LES turbulence modelling. The suitability of a LES turbulence model in combination with DGA lies in the concept being chosen for calculating turbulent viscosity. In this turbulence model, turbulent viscosity is proportional to the cell size of the element, therefore an increase in mesh resolution will lead to a reduction in local turbulent viscosity. In case of a very fine mesh the contribution of the LES turbulence model vanishes and the flow is practically calculated without turbulence model.

2.1. Dynamic grid adaptation

One method to reduce the numerical error is by reducing the size of the discretization elements. However, an excessive increase in mesh resolution would lead to insurmountable demand for computational power. As a consequence a mesh sensitivity analyses is required to find consensus in numerical error and computational demand. This requires the user to estimate before hand the regions of interest. Research has shown that the flow prediction is sensitive to the mesh resolution, this numerical behaviour indicates a need for dynamically generated mesh, which adapt the mesh to the flow field to cover interesting flow phenomena in high detail. A well developed and robust DGA algorithm can lead to a reduction in both numerical error and computational requirements. This appealing feature has encouraged the CFD society to develop a whole range of algorithms for DGA of different applicability and complexity.

2.1.1. Refinement strategies. In recent years a whole series of strategies have been developed, a small number of these strategies are preprocessing based and focus on a geometry based mesh refinement. For CFD purposes the majority of the strategies is focussing on a solution

based mesh refinement. This work will deal with the solution based mesh refinement. Three approaches can be distinguished;

R-refinement or grid movement (*relocation*): In this approach a basically fixed number of grid points is used, but the point positions are moved in such a way so that the grid points concentrate in critical spatial areas [8]. R-refinement plays an important and growing role in computational fluid dynamics, especially where the fluid interacts with moving walls (as in piston engines or structures yielding to an overpressure).

H-refinement in this approach a variable number of grid points is used. Points are added to, or removed from, the grid according to the local requirements, without changing the positions of the other grid points. As a result the grid is locally refined or coarsened [5].

P-refinement in this approach a principally fixed grid is used, but adaptive solution is obtained by locally varying the order of spatial discretization. Methods which do accomplish the addition of higher order shape functions are either the conventional polynomials [9], spectral element functions [10] or hierarchical shape-functions [11]. P-refining methods are increasingly used in finite-element methods, often together with h-refining methods [5].

2.1.2. Indication of error. In flow simulations the regions of interest will naturally be regions where there are strong gradients. The issue of grid refinement is to modify the grid and focus on the regions of interest.

The information about the regions where the grid should be refined or coarsened ideally should be provided by an error estimator. Error estimation for fluid flow calculations is not an easy task. The Navier–Stokes equations are a coupled, non-linear system and errors present in any one of these fields in general will effect the solutions of all others, in a non-linear manner difficult to describe accurately. The discretization error describes the deviation from the analytical solution of the set of differential equations, but is not directly accessible. However, it is possible to construct approximations to this error.

There are a number of adaptive methods in CFD which are designed to be used in combination with finite element, finite volume and finite difference schemes. The different schemes can be divided in four groups:

- Jump in property variable.
- Interpolation theory.
- Comparison of derivatives.
- Residue of partial differential equation.

2.2. LES turbulence model

The fluctuations occurring in the flow can be associated with a range of different turbulence scales, also known as eddies. The large scales are associated to low frequency vortices and their behaviour is dominated by the main flow. The small scales are more isotropic and uniform in their behaviour, consequently the effects of small scales are easier to estimate.

The idea behind LES turbulence modelling is to use a mesh fine enough to ensure that the larger scales can be resolved explicitly by the mesh, while the small scales—called subgrid scales—which cannot be observed in the numerical domain, are estimated via the LES model assumptions. The small scales are taken into account via an extra dissipation term, which accounts for the energy dissipation which occurs in the small scales.

For the turbulent flow computations the space averaged Navier–Stokes equations of an incompressible fluid are written as

$$\frac{\partial \overline{u_i}}{\partial t} + \overline{u_j}\frac{\partial \overline{u_i}}{\partial x_j} = -\frac{1}{\rho}\frac{\partial p}{\partial x_i} + \frac{(\mu_{\text{lam}} + \mu_t)}{\rho}\frac{\partial^2 \overline{u_i}}{\partial x_j \partial x_j} \tag{1}$$

Here the overbar represents the filtered variable. The term μ_t for the space averaged equation is called the subgrid scale viscosity or turbulent viscosity. Smagorinsky [12] proposed a method of calculating the subgrid scale viscosity as shown in Equation (2).

$$\mu_t = \rho l_s^2 |\bar{S}| \tag{2}$$

$$l_s = C_s \Delta \tag{3}$$

Here C_s is the Smagorinsky constant, which normally has a value in the range 0.10–0.25, Δ is the subgrid length scale associated to the grid size. The quantity $\bar{S}_{ij}$ is the resolvable strain rate given by Equation (4).

$$\bar{S}_{ij} = \frac{1}{2}\left(\frac{\partial \bar{u}_i}{\partial x_j} + \frac{\partial \bar{u}_j}{\partial x_i}\right) \tag{4}$$

In the next step the locally calculated turbulent viscosity, which for each element varies in magnitude, is added to the laminar viscosity. In the new time step, the governing equations will be resolved, including the turbulent viscosity to account for the subgrid scales.

2.2.1. Near wall treatment. For the LES simulation no wall function is used, but wall effects were taken into account by reducing the length scale in the vicinity of the cylinder surface. A damping variable D_{damp} was introduced to reduce the Smagorinsky constant in a region 20% of the cylinder diameter around the cylinder. The damping function has an alternative form to the standard van Driest damping function as shown in Equation (5). This was suggested by Tutar and Holdø [1] who indicated that the use of the standard van Driest wall function for separated flows, i.e. a flow passing a circular cylinder, is questionable.

$$D_{\text{damp}} = 1 - \mathrm{e}^{-(y^+/A^+)^2} \tag{5}$$

Here A^+ is a constant, which in accordance with literature, is assumed to be 25, y^+ is the distance of the element to the wall in terms of wall-shear units, i.e. $y^+ = yu_\tau/\nu$. The shear friction velocity u_τ is calculated from the velocity gradient at the wall, i.e. $u_{\tau=}\sqrt{\nu du/dy}$. Thus, by taking the wall effects into account, a damped value for the length scale is calculated in the wall region via $l_s = C_s \Delta D_{\text{damp}}$.

3. REACFLOW CFD SOLVER

For the simulations carried out in this work the CFD code REACFLOW [7] has been utilized. REACFLOW calculates the solution to the multicomponent, variable-density incompressible Navier–Stokes equations. The spatial discretization of the equations is based on an unstructured

triangular mesh. The primitive variables are all discretized in a cell-centred fashion, with one value for each variable in each triangular element. The variables are assumed to have a given functional dependency inside each element.

The pressure p is discretized in a vertex-centered fashion, where each pressure value is defined on a *control volume*, delimited by the medians in all the triangles surrounding the given vertex. This choice of discretization has been made to suppress the 'checkerboard' instability.

For incompressible flows the velocity must satisfy the divergence-free criterion: $\partial u_i/\partial x_i = 0$. This introduces an extra constraint which replaces the traditional equation of state. It also makes the sound speed infinite, so a degree of implicitness must be employed in the timestepping.

The numerical method used is similar to the predictor–corrector method of Chorin [13]. The solutions to the equations for mass, mass fractions and internal energy are all advanced in an explicit fashion.

For the velocity, an intermediate state, u_i^* is found by advancing all the terms except the pressure gradient term explicitly. A Poisson equation is then found for the pressure by taking the divergence of the velocity equation:

$$\frac{\partial u_i^{n+1}}{\partial x_i} = \frac{\partial u_i^*}{\partial x_i} - \frac{\Delta t}{\rho^{n+1}} \frac{\partial}{\partial x_i} \left(\frac{\partial p^{n+1}}{\partial x_i} \right) \tag{6}$$

The final velocity must be divergence-free, so the term on the left-hand side of Equation (6) vanishes.

The solver uses a numerical discretization method very similar to a finite-volume method, where the unknowns are the integrals of the primitive variables over each element. The contributions from the advective terms may then be calculated as an integral over the element boundary of the fluxes, denoted as $\bar{w}_j \equiv \int_{\Omega_j} w(x_i)\,\mathrm{d}V/|\Omega_j|$. For a given element Ω and a given field w this gives:

$$\int_\Omega u_i^n \frac{\partial w^n}{\partial x_i}\,\mathrm{d}V \simeq u_i^n \int_\Omega \frac{\partial w^n}{\partial x_i}\,\mathrm{d}V = u_i^n \int_{\partial\Omega} n_i w^n\,\mathrm{d}S \tag{7}$$

where the Green's theorem is used to obtain the surface integral in the last equality.

The finite-volume formulation gives values for the integral over the elements of the primitive variables. In order to calculate the surface integrals of Equation (7) a function $\tilde{w}_j(x_i)$ for w must be found in Ω_j such that $\int_{\Omega_j} \tilde{w}_j\,\mathrm{d}V = |\Omega_j|\overline{w_j}$.

If $\tilde{w}_j(x_i)$ is assumed constant (equal to $\bar{w}_j$), the resulting numerical scheme will be first-order accurate in space. Choosing a linear dependency in space for $\tilde{w}_j$ nearly second-order accuracy in space can be obtained. To find the associated constant gradient the gradient of w in the control volumes is determined. This can be found using Green's theorem over the control volume boundary, using the (assumed constant) values of w inside each element touching the control volume. The gradient in the element may then be found by the following rule:

$$|w|_e = \begin{cases} k \min_{\mathrm{CV}|e} |w|_{\mathrm{CV}|e} & \text{if } k \min_{\mathrm{CV}|e} |w|_{\mathrm{CV}|e} < \min^*_{\mathrm{CV}|e} |w|_{\mathrm{CV}|e} \\ \min^*_{\mathrm{CV}|e} |w|_{\mathrm{CV}|e} & \text{if } k \min_{\mathrm{CV}|e} |w|_{\mathrm{CV}|e} > \min^*_{\mathrm{CV}|e} |w|_{\mathrm{CV}|e} \end{cases} \tag{8}$$

where $\min_{\mathrm{CV}|e}$ is the minimum over the control volumes touching element e, and $\min^*$ is the minimum of all the values but the minimum (i.e. the second-smallest value). If $k = 1$

the minimum of the gradients in the control volumes is always chosen. This corresponds to the *minmod* limiter [14]. In order to preserve the total variation diminishing (TVD) property it must be demanded that $k \leqslant 2$, with $k = 2$ corresponding to the *Superbee* limiter [14]. The minmod limiter is the most diffusive one, but possibly yields the more robust numerical solutions, whereas the superbee limiter yields sharper profiles near discontinuities. To minimize the numerical diffusion in order not to mask the effects of turbulent viscosity Roe's superbee limiter was selected.

4. SOFTWARE DEVELOPMENT

4.1. Dynamic grid adaptation

The refinement strategy being used in the REACFLOW code is the so-called h-refinement, where grid points are added and removed based on the error estimation and the error bounds, defined at the start of the simulation. The refinement of the mesh always takes place across the longest edge of the triangular element, which ensures that triangles with very high aspect ratio are not formed.

4.1.1. Method for error indication. The method for error indication implemented is an estimation of the local interpolation error. For a given variable of interest, q, an interpolated value for a grid point x_i can be defined. This value $\hat{q}_i$ can be defined in various ways. However, in the present work the arithmetical mean is defined over the neighbour grid points:

$$\hat{q}_i \equiv \frac{1}{N} \sum_{j=1}^{N} q_j \tag{9}$$

where q_j are the values of the variable at the jth of the N neighbours of the grid point x_i. The interpolated value may now be compared with the actual value in that grid point, q_i. If the absolute value of the difference

$$e_i \equiv |q_i - \hat{q}_i| \tag{10}$$

is greater than a predefined value, a new grid point will be inserted in the vicinity.

An error estimation of this kind assumes the solution to be smooth and will lead to mesh refinement in the region where there is a variation in the refinement variable. An advantage of the interpolation method, in comparison to other methods, is that all neighbour elements are included in the determination of a new node, leading to a smoother mesh refinement.

4.1.2. Refinement variable. The determination of an appropriate refinement variable to approximate the discretization error depends very much on the physical problem investigated. Widely used refinement variables in this respect are the density, pressure and velocity gradients, as well as the turbulent viscosity. However, the discretization error describing the deviation from the analytical solution of the set of differential equations is not directly accessible. Therefore, the refinement variable is a compromise between the quality of the error indication and the computational complexity of the refinement variable.

Modification to turbulent viscosity as a refinement variable: The variable used in this work is derived from the equation for turbulent viscosity in the LES turbulence model. By

varying the weight of either the cell size or the strain rate, by means of the DGA variables C_m and C_{str}, a different adaptation behaviour can be established. The DGA variables C_m and C_{str} have to be defined at the start of the simulation, and are constant throughout the domain. An increase of the variable C_m will lead to a more solution independent mesh refinement, while an increase in the variable C_{str} will lead to a mesh refinement in the regions where high velocity gradients exist.

$$q_i = \rho C_s^2 \Delta^{C_m} |\bar{S}|^{C_{str}} \tag{11}$$

4.2. Turbulence model

Modelling turbulent flow with the Standard Smagorinsky LES turbulence model requires the implementation of Equation (2). This equation calculates the subgrid scale viscosity by means of four parameters:

- Subgrid length scale Δ.
- Density ρ.
- Smagorinsky constant C_s.
- Rate of strain $|\bar{S}|$.

Both density and rate of strain can be obtained from the CFD code, while the Smagorinsky constant can be set to 0.15, as suggested in literature [12, 15]. Extra attention was given to the definition of subgrid length scale, because of the triangular shape of the elements.

Subgrid length scale: A widely used definition for the subgrid length scale in 2-D rectangular mesh is $\Delta = \sqrt{\Delta_x \Delta_y}$, nevertheless in several studies it was found that $\Delta = \sqrt{2\Delta_x \Delta_y}$ leads to more accurate results than $\Delta = \sqrt{\Delta_x \Delta_y}$ [16] and in some cases even $\Delta / \sqrt{\Delta_x \Delta_y} > 2$ seems necessary [17]. In the work of Vreman *et al.* [16] the subgrid length scale Δ in LES was set equal to $\Delta = \sqrt{2\Delta_x \Delta_y}$, indicating that a minimum of two elements is taken to represent the smallest eddies resolved in the flow field. In other words, what is the minimum grid being necessary for resolving a turbulent scale in a triangular unstructured mesh. The smallest possible scale to be modelled employs three grid point, in such case the length scale is defined as the square root of the element surface. However, it is questionable if three grid points are sufficient to model a turbulent scale and therefore a second definition for the subgrid length scale is proposed. In the second definition twice the surface area is used for the subgrid length scale, which implies four grid points are required to model a turbulent scale properly.

The first definition for the subgrid length scale is based on the surface area of the element and reads:

$$\Delta = \sqrt{\frac{\Delta_x \Delta_y}{2}} = \sqrt{A_{tr}} \tag{12}$$

In the second definition for subgrid length scale a conventional definition is utilized which reads:

$$\Delta = \sqrt{\Delta_x \Delta_y} = \sqrt{2A_{tr}} \tag{13}$$

This definition suggests that two elements are required for resolving a turbulent scale. Compared to $\Delta = \sqrt{A_{tr}}$, LES results obtained with $\Delta = \sqrt{2A_{tr}}$ are less sensitive to discretization errors. A larger $\Delta / \sqrt{A_{tr}}$ ratio leads to smaller discretization errors, but on the other hand the

$\Delta/\sqrt{A_{\text{tr}}}$ ratio is required to be as small as possible in order to retain a maximum amount of information in the resolved scales.

5. SIMULATION RESULTS AND DISCUSSIONS

5.1. Computational domain and simulations

The computational domain and boundary conditions used for the simulations with DGA are shown in Figure 1(b) shows the mesh at the start of the simulation. At the inlet boundary a uniform velocity profile is imposed, while on the outlet boundary pressure is imposed and velocity is set free. No-slip boundary conditions are applied to the cylinder wall and all velocity components are set to zero. On both horizontal boundaries velocity is imposed; the velocity in the y direction is set to $v=0$ so that no flow can be drained off or entrained via these boundaries. To ensure no mesh refinement will take place along the horizontal boundaries, the x-component of the velocity is set equal to the velocity imposed at the inlet in order not to maintain any velocity gradient along the horizontal boundaries.

In this work a total of seven simulations were carried out. The first two simulations presented are carried out with conventional mesh using 6.1×10^4 nodes and a subgrid length scale $\Delta=\sqrt{A_{\text{tr}}}$ and $\sqrt{2A_{\text{tr}}}$, respectively. The other five simulations have utilized the DGA algorithm. The configuration of the DGA algorithm required specification of the DGA variables C_{m} and C_{str}, threshold values for mesh refinement and coarsening, as well as a minimum mesh size to restrict excessive mesh refinement. Details of the DGA configuration are presented in Table II.

The flow profiles shown are the time integrated streamwise velocity component both in streamwise and transverse direction, as well as the turbulent shear stress along the transverse axis. In addition drag coefficient $C_D^{\ddagger}$, Strouhal number $S_t^{\S}$ and separation angle are calculated from the time integrated flow field and presented in Table I.

The existence of periodic waves, as well as motions associated with turbulence in the flow field, requires the data to be integrated in time so as to obtain flow features associated to time integrated values obtained by experiments [18]. The flow in the near wake can be viewed formally as a combination of a global mean component $\bar{s}$, a periodic component $\tilde{s}$, and a fluctuating component s', where s is any variable. By definition the total variable s is the sum

$$s=\bar{s}+\tilde{s}+s' \tag{14}$$

The mean component is calculated by an averaging process, as shown in Equation (15),

$$N\bar{s}=\sum_{n=1}^{N} s_n \tag{15}$$

while the periodic motions are distinguished from the turbulent motion via a fast fourier transform (FFT). The fluctuating component s' which remains is associated with turbulence and can be used to calculate the Reynolds stresses $\overline{u_i'u_j'}$.

‡The drag coefficient is the sum of the streamwise pressure forces acting on the cylinder relative to the density and inlet velocity $C_D=2F_D/\rho u_\infty^2$.

§Strouhal number is the frequency of the periodic wave relative to cylinder diameter and inlet velocity $S_t=fD/u_\infty$.

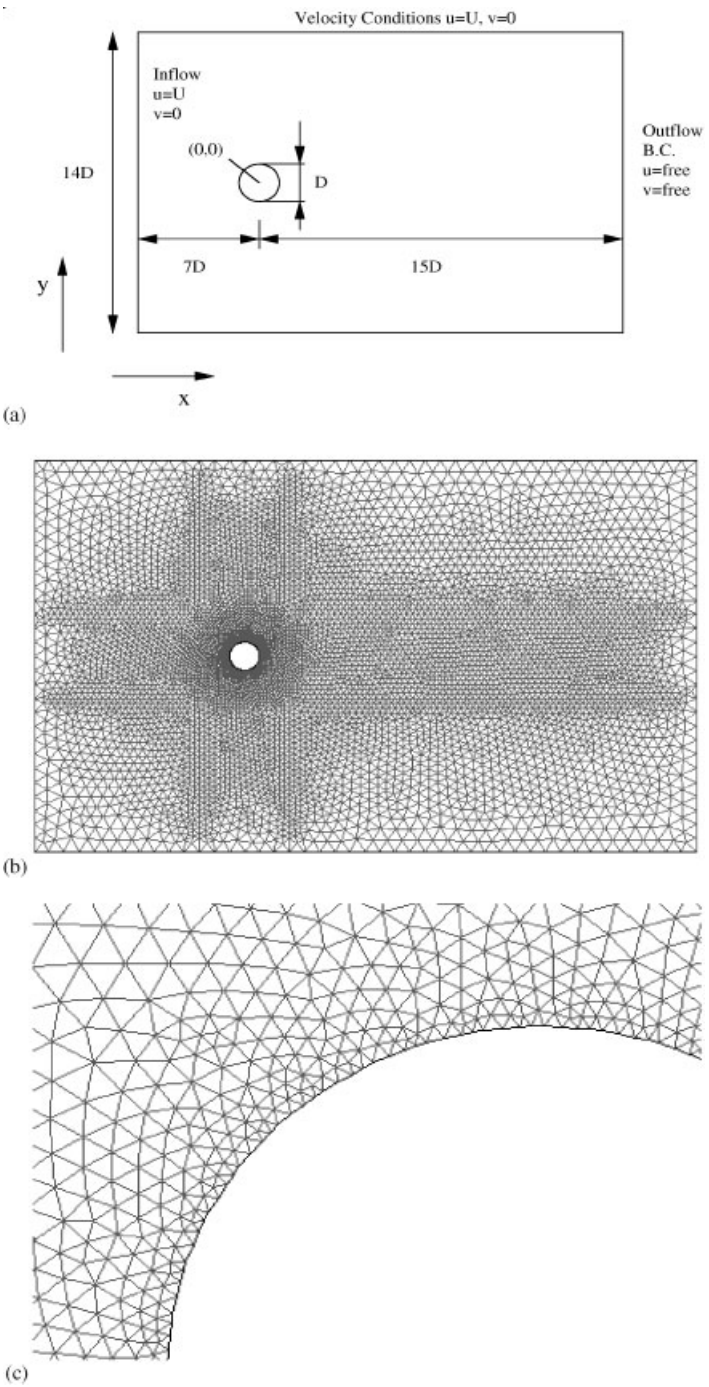

Figure 1. Dimensions of simulation model and initial mesh: (a) dimensions in ratio of cylinder diameter; (b) initial mesh containing 7500 nodes; (c) initial mesh near the wall.

Table I. Flow parameters for a circular cylinder at $Re = 1.4e5$.

	C_D	S_t	Separation angle (deg)
Reference [18]	1.24	0.179	77
$l_s = C_s\sqrt{A_{tr}} \mid \text{nodes} = 6.1 \times 10^4$	—	0.174	86
$l_s = C_s\sqrt{2A_{tr}} \mid \text{nodes} = 6.1 \times 10^4$	—	0.160	90
$C_m = 1 \mid C_{str} = 1 \mid \text{nodes} = 2.8 \times 10^4$	1.45	0.180	96
$C_m = 1 \mid C_{str} = 1 \mid \text{nodes} = 4.3 \times 10^4$	1.47	0.188	89
$C_m = 1 \mid C_{str} = 1 \mid \text{nodes} = 4.5 \times 10^4$	1.35	0.210	95
$C_m = 1 \mid C_{str} = 2 \mid \text{nodes} = 1.4 \times 10^4$	1.46	0.173	81
$C_m = 1 \mid C_{str} = 2 \mid \text{nodes} = 2.8 \times 10^4$	1.38	0.176	85

Table II. Configuration of DGA algorithm.

$C_m \mid C_{str} \mid$ nodes	Upper threshold	Lower threshold	Max. mesh resolution $(1/A_{tr})$
$C_m = 1 \mid C_{str} = 1 \mid 2.8 \times 10^4$	5.0×10^{-4}	2.50×10^{-4}	2.44×10^5
$C_m = 1 \mid C_{str} = 1 \mid 4.3 \times 10^4$	2.5×10^{-4}	1.25×10^{-4}	2.44×10^5
$C_m = 1 \mid C_{str} = 1 \mid 4.5 \times 10^4$	2.5×10^{-4}	1.25×10^{-4}	9.80×10^5
$C_m = 1 \mid C_{str} = 2 \mid 1.4 \times 10^4$	7.0×10^{-4}	3.50×10^{-4}	2.44×10^5
$C_m = 1 \mid C_{str} = 2 \mid 2.8 \times 10^4$	3.5×10^{-4}	1.75×10^{-4}	2.44×10^5

5.2. *Basic flow features*

In this work a variety of simulations is presented and compared with the experimental data from Cantwell and Coles [18]. Although the comparison of simulation results and experimental data is crucial to validate the flow field, a critical remark has to be added here. It is well known that the flow around a cylinder is not only dependent on the Reynolds number, but on a variety of influencing factors. The most important ones are the ratio between cylinder diameter and cylinder length, the blockage ratio of the cylinder, the end conditions, the roughness of the cylinder and the free-stream turbulence level. This typically leads to highly scattered experimental data such as the data collection by Cantwell and Coles [18] for the drag coefficient and the Strouhal number demonstrates. Therefore differences between experimental conditions and the simulation results are apparent. The most relevant ones in this investigation are the 2-D simplification and the zero turbulence level at the inflow, which is not feasible in wind or water tunnel experiments.

The results obtained from the simulations using DGA as well as a conventional mesh show strong variation in the flow prediction. The dimensions of the wake region behind the cylinder, as well as the turbulence intensity along the transverse axis are predicted with varying success, as shown in Figures 2–10. For the simulations using DGA the recirculation region is predicted to be half the cylinder diameter in most of the simulations which agrees with the experimental data. Only an exceptional deviation with experimental data is apparent in the simulation with C_m and C_{str} being both 1 and a mesh containing 2.8×10^4 nodes; here the recirculation region is predicted to be a quarter of the cylinder diameter. The small dimensions of the recirculation region are confirmed by the separation angle which is predicted

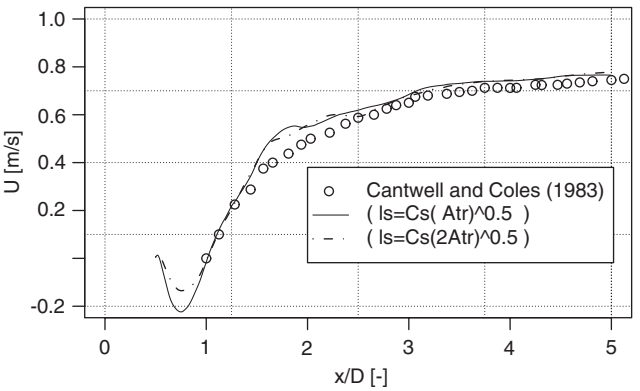

Figure 2. Time averaged normalized velocity along streamwise axis at $y/D=0$, for simulations using conventional mesh with 6.1×10^4 nodes.

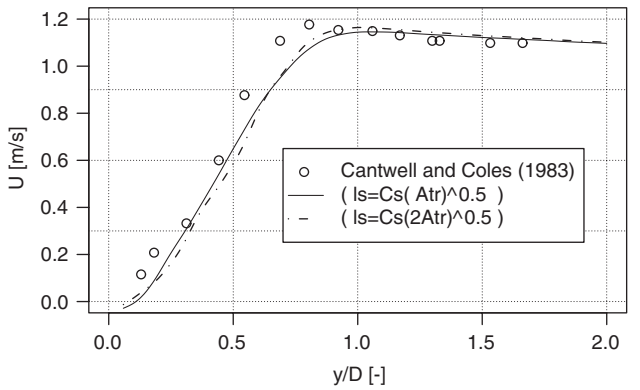

Figure 3. Time averaged normalized velocity along transverse axis at $x/D=1$, for simulations using conventional mesh with 6.1×10^4 nodes.

to be 96°, an over prediction of 19° in the separation angle indicates a narrow wake. As the wake is decreasing in size a reduction in drag coefficient would be expected, nevertheless the drag coefficient is predicted to be 1.47 in the simulation with C_m and C_{str} being both 1 and mesh containing 2.8×10^4 nodes. The over prediction of drag coefficient is typical for most of the simulations presented and is also shown in previous work of Tutar and Holdø [1] and Breuer [2].

The velocity decay is predicted well for the simulations using $C_m=1$ and $C_{str}=2$, however there is a lack of agreement in the simulation with C_m and C_{str} being 1 and 2, respectively and a mesh containing 2.8×10^4 nodes, in the region 3–5 cylinder diameters away from the cylinder. Similarly, the downstream region deviates from experimental data in the simulations with a mesh containing 4.3×10^4 and 4.5×10^4 nodes, respectively, indicating a short wake region. Both simulations have over predicted the Strouhal number with 5 and 17%, respectively, while in all other simulations Strouhal number is predicted in good agreement with experimental data. Surprisingly the deviation with experimental data grows with increasing

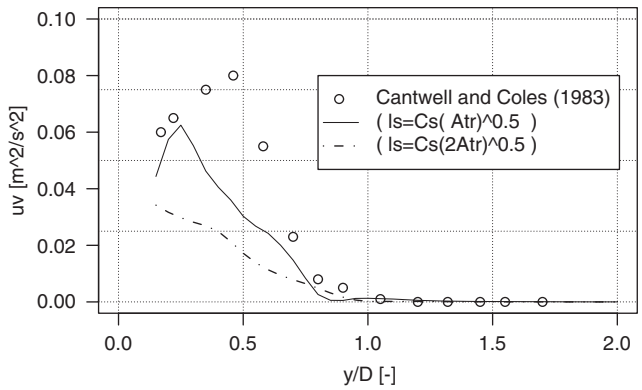

Figure 4. Time averaged normalized shear stress due to turbulence along transverse axis at $x/D=1$, for simulations using conventional mesh with 6.1×10^4 nodes.

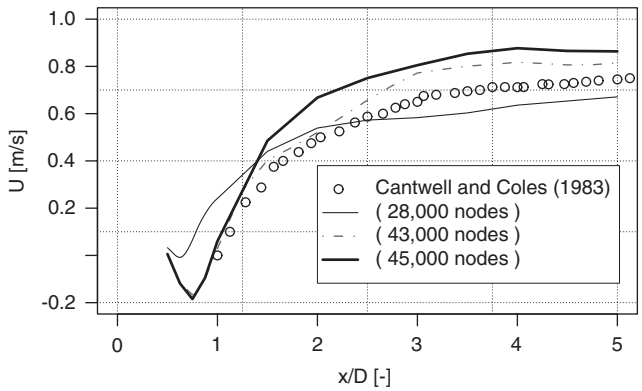

Figure 5. Time averaged normalized velocity along streamwise axis at $y/D=0$, for simulations using DGA constants $C_{\mathrm{m}}=1-C_{\mathrm{str}}=1$.

mesh resolution. The prediction of turbulent shear stress in the wake region confirms that an increase in mesh resolution does not automatically lead to an improvement of the flow prediction. Although there is a clear trend that an increasing mesh resolution leads to an increase in shear stress, the simulation using a mesh of approximately 4.5×10^4 nodes does over predict the shear stress by about 25%. A reduction in quality of the prediction with increasing mesh resolution was not expected beforehand. Nevertheless, trends of this kind where also seen in the work of Breuer [2]. Distinct arguments for these trends are difficult to present as this problem relates to the resolution of small scale vortices of the small scale flow phenomena.

5.3. *Effects of the subgrid length scale*

A comparison of the two simulations, using conventional mesh, with the experimental data from Cantwell and Coles [18] shows that the average velocity field is predicted well in both simulations. For turbulent shear stress, Strouhal number and separation angle there is less

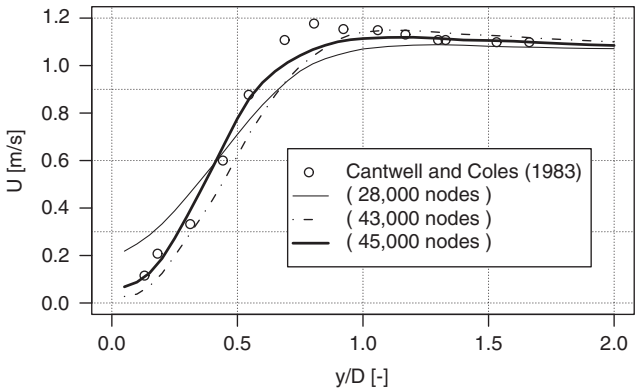

Figure 6. Time averaged normalized velocity along transverse axis at $x/D=1$, for simulations using DGA constants $C_m=1-C_{str}=1$.

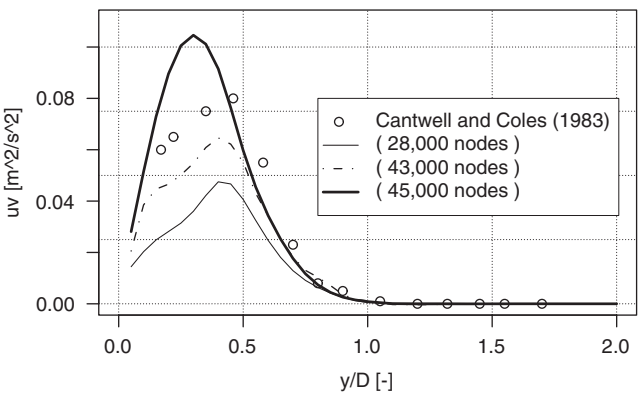

Figure 7. Time averaged normalized shear stress due to turbulence along transverse axis at $x/D=1$, for simulations using for simulations using DGA constants $C_m=1-C_{str}=1$.

agreement with experimental data. The turbulent shear stress profiles do indicate that turbulent viscosity is over predicted with the second subgrid length scale ($\Delta=\sqrt{2A_{tr}}$) and that initial instabilities in the flow field are diffused. For Strouhal number and separation angle there is a growing deviation from experimental data when applying the second definition for subgrid length scale. Based on the results of both simulations and the deviation with experimental data it is concluded that a better flow field is obtained with the subgrid length scale ($\Delta=\sqrt{A_{tr}}$). For this reason the remaining simulations with DGA were carried out with the first definition for subgrid length scale.

5.4. Influence of grid adaptation constants C_m and C_{str}

With the introduction of the two variables C_m and C_{str} in the refinement variable there is a user defined control. The use of the adaptation constants for the grid adaptation is clearly shown in Plates 2 and 3. In the first figure a smooth mesh refinement has taken place in the shear

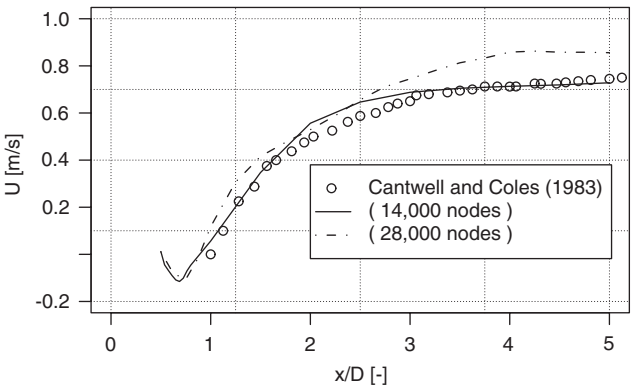

Figure 8. Time averaged normalized velocity along streamwise axis at $y/D=0$, for simulations using DGA constants $C_{\mathrm{m}}=1-C_{\mathrm{str}}=2$.

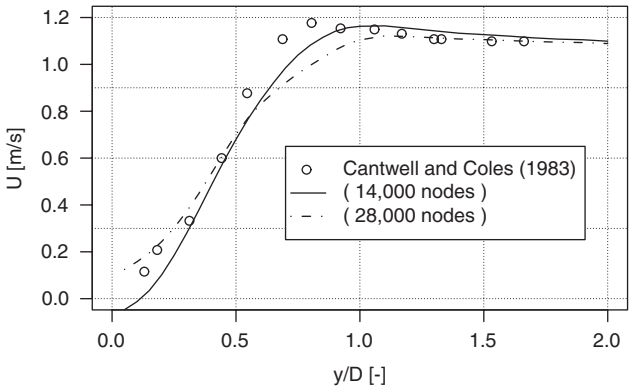

Figure 9. Time averaged normalized velocity along transverse axis at $x/D=1$, for simulations using DGA constants $C_{\mathrm{m}}=1-C_{\mathrm{str}}=2$.

layers and along the cylinder, while in the latter the refinement is sharp and narrow and more focussed on areas that maintain a high rate of strain. Therefore, despite the limited number of nodes in the simulation with $C_{\mathrm{m}}=1$, $C_{\mathrm{str}}=2$ and 1.4×10^4 nodes, its smallest element (Table III) is still smaller than the equivalent element (Table III) in the simulation with $C_{\mathrm{m}}=1$, $C_{\mathrm{str}}=1$, and 2.8×10^4 nodes, as shown in Table III. The effect of the adaptation constants is seen particularly well in the vortices and the surrounding area as shown in Figure 11.

The variation in flow prediction is primarily due to mesh refinement and confirms the complexity of the physical processes in which certain flow regions and vortex scales in the flow field are over proportionally important. This means that the determination of a proper refinement variable can not be decoupled from the physics that are under investigation. A good refinement variable for separating flows at high Reynolds numbers is not by definition suitable for flows where other features are of key interest. Nevertheless, it would be expected that a high level of mesh refinement is only required in limited areas.

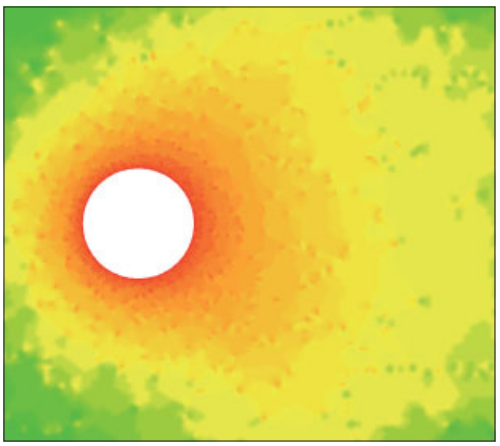

Plate 1. Mesh resolution ($\log 1/A_{\mathrm{tr}}$) around circular cylinder for simulations using conventional mesh with 61 000 nodes.

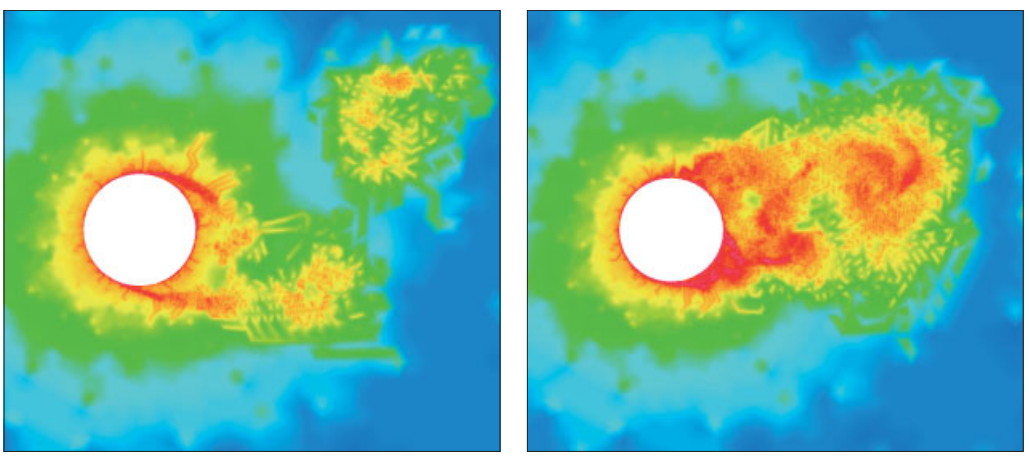

(a) (b)

Plate 2. Instantaneous mesh resolution ($\log 1/A_{\mathrm{tr}}$), in fully developed flow around circular cylinder for simulations using DGA constants $C_{\mathrm{m}} = 1 - C_{\mathrm{str}} = 1$: (a) 14 000 nodes; (b) 28 000 nodes.

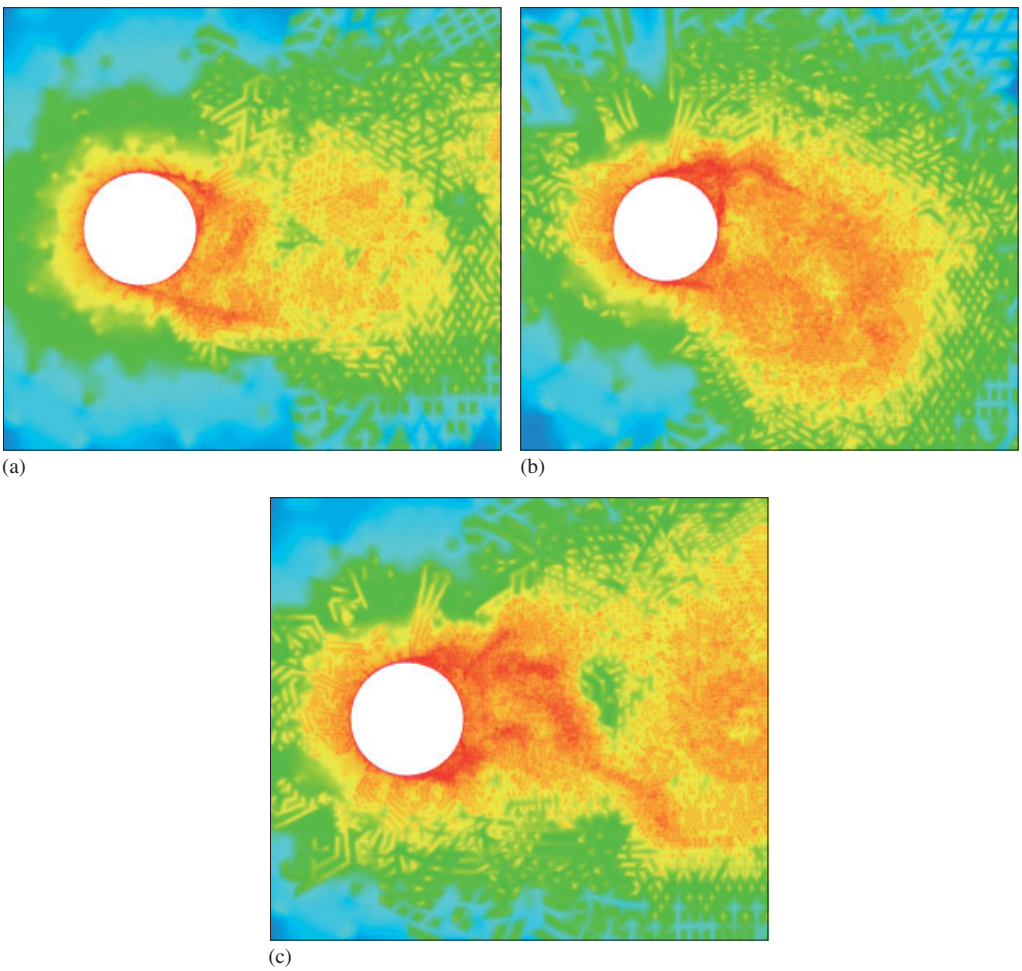

Plate 3. Instantaneous mesh resolution ($\log 1/A_{\mathrm{tr}}$), in fully developed flow around circular cylinder for simulations using DGA constants $C_{\mathrm{m}} = 1 - C_{\mathrm{str}} = 2|$ (a) 28 000 nodes; (b) 43 000 nodes; (c) 45 000 nodes.

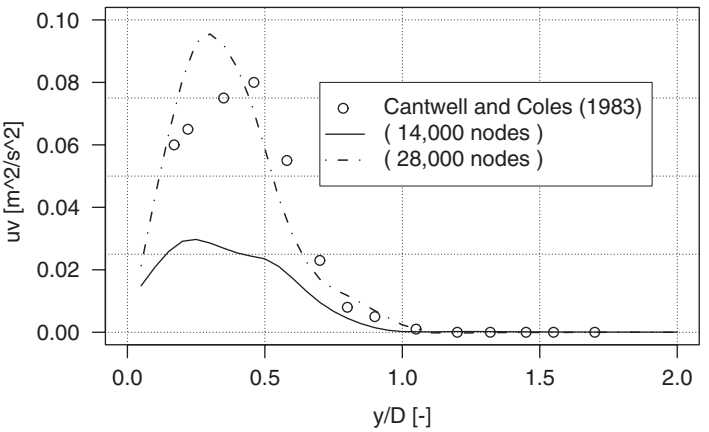

Figure 10. Time averaged normalized shear stress due to turbulence along transverse axis at $x/D=1$, for simulations using for simulations using DGA constants $C_m=1-C_{str}=2$.

Table III. Maximum mesh resolution for a circular cylinder at $Re=1.4e5$.

	Max. mesh resolution $(1/A_{tr})$
NO-DGA | nodes $=6.1\times10^4$	7.20×10^4
$C_m=1 \mid C_{str}=1 \mid$ nodes $=2.8\times10^4$	1.18×10^5
$C_m=1 \mid C_{str}=1 \mid$ nodes $=4.3\times10^4$	1.55×10^5
$C_m=1 \mid C_{str}=1 \mid$ nodes $=4.5\times10^4$	4.72×10^5
$C_m=1 \mid C_{str}=2 \mid$ nodes $=1.4\times10^4$	1.55×10^5
$C_m=1 \mid C_{str}=2 \mid$ nodes $=2.8\times10^4$	1.58×10^5

From the perspective of mesh correlation it is interesting that the flow field predicted in the simulation with $C_m=1$, $C_{str}=2$ and a mesh containing 1.4×10^4 nodes has obtained not only good agreement with experimental data, but also with the simulation using conventional mesh and a subgrid length scale $\Delta=\sqrt{A_{tr}}$. Both simulations do maintain similar mesh resolution in the vicinity of the wall and shear layer, the only significant difference lies in the prediction of turbulent shear stress towards the centreline. It could be argued that the lack of agreement in turbulent shear stress occurs due to the coarse mesh away from the cylinder in the region where the shear stress profile is located (Plate 1).

Despite the fact that in the simulation with $C_m=1$, $C_{str}=1$ and 4.3×10^4 nodes, velocity decay, drag coefficient and separation angle are predicted with considerable error there is a surprisingly good agreement in trend and magnitude of the shear stress profile. Although none of the flow profiles and flow parameters can be seen in isolation it is worth noticing that the inclusion of small scale vortices in the vicinity of the wall, as in the simulation with $C_m=1$, $C_{str}=1$ and 4.5×10^4 nodes, will lead to an increase in turbulent shear stress, as well as a deformation of the stress profile giving its peak stress at 0.3 cylinder diameters from the centreline. The deformation of the stress profile means that there is a displacement of turbulent activity towards the centreline. The displacement of turbulent activity suggests that due to lower threshold values relatively more turbulent motions along the centreline are

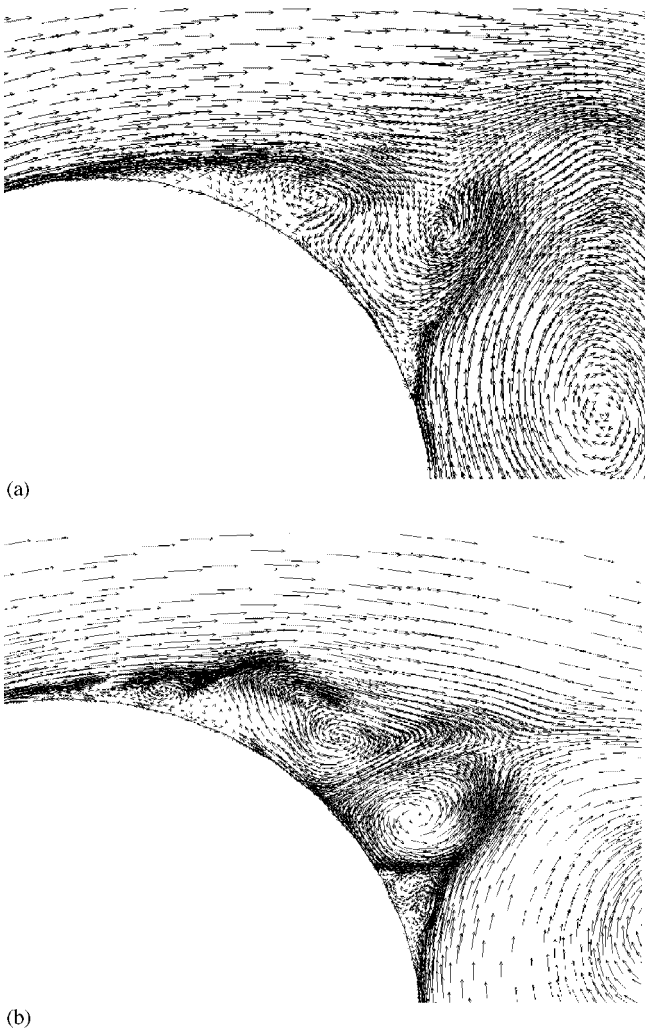

Figure 11. Instantaneous vector plot of flow in the vicinity of the wall: (a) $C_m = 1|\ C_{str} = 1|$ 45,000 nodes; (b) $C_m = 1|\ C_{str} = 2|$ 28,000 nodes.

captured. The region along the centreline is thus more sensitive to sharper mesh refinement conditions in comparison with the outer region. This idea is confirmed by Plates 2 and 3,

which show that the bulk of the additional refinement is allocated in the recirculation region between the upper and lower shear layer.

The lack of shear stress near the centreline in the simulation with $C_m = 1$, $C_{str} = 1$, and 2.8×10^4 nodes, should be considered with respect to the mesh resolution at one diameter away from the centre of the cylinder. In this region mesh resolution is only a fraction in comparison with the simulation using conventional mesh. Therefore the importance of these vortices for the flow field is subject to discussion and the simulations indicate that the important flow mechanisms where the flow will be determined take place further upstream, in the vicinity

of the wall, separation point and shear layers. It is in these narrow regions where high mesh resolution is required, therefore a better mesh adaptation is accomplished by using $C_m = 1$ and $C_{str} = 2$. Here substantially less nodes are used in comparison with the simulations using $C_m = 1$ and $C_{str} = 1$, while better agreement is obtained with the experimental data.

Despite the support for the hypothesis being presented here, it is interesting to note that a further mesh refinement in the vicinity of the wall does not improve the flow prediction. A decay in the quality of the prediction could occur due to separation taking place in turbulent mode, however the thin boundary layer up to the point of separation is resolved by about 6–10 elements and this number is smaller then in the work of Tutar and Holdø [1] and Breuer [2] who used 15 and 25 grid points, respectively. There is no turbulent kinetic energy until the point of separation which suggests that separation takes place in the laminar mode as experimentally expected for a sub-critical Reynolds numbers forming free shear layers. It is only in the separation point and shear layers where the mesh resolution exceeds the resolution used in the work of Tutar and Holdø [1] and Breuer [2]. In this region the shear layer contains about 30 elements in radial direction, while in clockwise direction the mesh resolution is about 3 elements per degree. In comparison, Tutar and Holdø and Breuer used 0.5 and 1 element per degree respectively. The reason for strong mesh refinement in clockwise direction, is because mesh refinement in the element always takes place over the longest edge, leading to equilateral shaped elements. As a consequence small scale isotropic vortices are modelled, which do not exist neither in the simulations with C_m and C_{str} to be 1 and 2, respectively, and a mesh containing 1.4×10^4 and 2.8×10^4 nodes nor in the work of Tutar and Holdø [1] and Breuer [2]. It is a plausible conjecture that the small scale vortices of this type, generated in the vicinity of the wall, lead to an increase in turbulent activity in the shear layers. As the vortices in the shear layer are growing in magnitude due to coalescing with surrounding vortices there will be an increase in turbulent intensity as supported by Figures 7–10. It is suggested by Richardson [19], who investigated the interaction between scales of different size, that the scales which are comparable in size with the scales in the separation region are effective in increasing the separation. Consequently, a different flow field is predicted due to a large number of scales in the wake region. The major question relevant to this conjecture is the physical representation of the small scale vortices. Although the numerics are inextricably bound up with the physics to be modelled, numerical requirements have to be fulfilled to ensure numerical stability of the flow field. To fullfill these criteria imperfections in the numerical scheme have to be accepted. In this respect it is important to mention the flux limiter used to ensure the TVD criteria. The existence of sharp velocity profiles makes the flow field more sensitive to dispersion in the flow field [14] leading to numerical dispersion. Another aspect relevant to the modelling of the flow field is the two-dimensional simplification in this work, as a consequence flow motions in the spanwise direction, which are expected to occur in real live are not considered. Therefore, the effect of three-dimensional flow motions on the flow prediction is subject to discussion and is an interesting point for further investigation.

6. CONCLUSION

The conventional meshes used in previous investigations have significant drawbacks. Due to the fact that the mesh is fixed throughout the simulation, a high mesh resolution has to

be applied in all regions where complex flow behaviour is expected. It is most likely that a significant percentage of the mesh will have only a marginal influence onto the flow prediction, leading to an inefficient use of the nodes. Therefore a proper design of the mesh requires a good understanding of the fluid dynamics being investigated, in particular if the flow is of high complexity as in flows for industrial application for example. Therefore, there are several advantages in using the DGA algorithm in flows for industrial application.

- A solution based grid refinement will minimize the need to estimate the flow field beforehand. This aspect of DGA is shown in Plates 2 and 3. The mesh generated towards the end of the simulation reflect the flow structures being modelled.
- There is no need for time consuming mesh testing

Despite the potential of DGA to use computational power more efficient, a reliable grid refinement thus depend on a proper error estimation which reflects the need for mesh refinement. The present work also shows that the success of adaptive grid strategies depends significantly on a reliable error estimation and on the adequate determination of acceptable error bounds. The importance of reliable error estimation and determination of error bounds on the flow prediction is shown in Figures 5–10 and Table I. The present work demonstrates that using a modified μ_t yields reliable results. A comparison of the simulations using DGA shows that an increasing number of nodes does not lead to improvement of the flow prediction. Instead, by using the flow prediction as a measure for the quality of mesh refinement, the highest quality of mesh is obtained in the simulation where $C_m = 1$, $C_{str} = 2$ and the number of grid points were 1.4×10^4. Here a strong, but narrow mesh refinement has taken place in the vicinity of the wall near the point of separation and in the small scale vortices in the shear layers further downstream, while a coarse mesh is maintained in the wake region behind the cylinder. It is encouraging that the results of this simulation compare well with the simulations using conventional mesh. Further results of the use of DGA in simulation with $C_m = 1$, $C_{str} = 2$ and a mesh containing 1.4×10^4 nodes are:

- A reduction in nodes of approximately 75% and a mesh resolution in the refined areas which is of equal order to the simulation using conventional mesh.
- The predicted flow parameters and averaged velocity profiles are in good agreement with each other, nevertheless the main differences between both simulations, can be found in the turbulent shear stress profiles along the transverse axis as shown in Figures 7 and 10.

Both conventional mesh and DGA based simulations under predict the shear stress near the centreline, but compare well with experimental results away from the centreline. Although the limitations with DGA in tracking the smaller scale vortices cannot be neglected, the majority of flow parameters and flow profiles are in agreement with experimental data.

NOMENCLATURE

A_{tr} element surface
A^+ constant
C_d drag coefficient
C_m adaptation constant for mesh

C_s	Smagorinsky constant
C_{str}	adaptation constant for strain
D	cylinder diameter
D_{damp}	damping variable
e_i	estimated error
l_s	length scale
n	instantaneous number of time step
N	number of neighbour elements
p	pressure
q	refinement variable
$\hat{q}_i$	interpolated refinement variable
Re	Reynolds number
S	volume of discretization element
$\|\bar{S}\|$	magnitude of strain
S_{ij}	strain tensor
S_t	Strouhal number
t	time
u	streamwise velocity component
u^*	streamwise intermediate velocity component
u_i	u, v, w for $i=1,2,3$, respectively
u_i^*	u^*, v^*, w^* for $i=1,2,3$, respectively
$\bar{u}$	average velocity
$\bar{u}_{cl}$	average centerline velocity
u'	streamwise fluc. velocity component
u_τ	shear friction velocity
v	lateral velocity component
V	surface of discretization element
v'	lateral fluc. velocity component
x	space in streamwise direction
x_i	x, y, z for $i=1,2,3$, respectively
y	space in lateral direction
y^+	distance in wall shear units
Δ	subgrid length scale
Ω	discretization element
μ_{lam}	laminar viscosity
μ_t	turbulent viscosity
ν	kinematic viscosity
ρ	density

REFERENCES

1. Tutar M, Holdø AE. Computational modelling of flow around a circular cylinder in sub-critical flow regime with various turbulence models. *International Journal for Numerical Methods in Fluids* 2001; **35**:763–784.
2. Breuer M. A challenging test case for large Eddy simulation: high Reynolds number circular cylinder flow. *International Journal of Heat and Fluid Flow* 2000; **215**:648–654.
3. Eiseman PR. Adaptive grid adaptation. *Computational Methods in Applied Mechanics and Engineering* 1987; **64**:321–376.

4. Habashi WG, Dompierre J, Bourgault Y, Yahia DAA, Fortin M, Vallet MG. Anisotropic mesh adaptation: towards user-independent, mesh-independent and solver-independent cfd. part 1: general principles. *International Journal for Numerical Methods in Fluids* 2000; **32**:725–744.
5. Lohner R. Mesh adaptation in fluid mechanics. *Engineering and Fracture Mechanics* 1995; **50**(5–6):819–847.
6. Muzaferija S, Gosman D. Finite-volume cfd procedure and adaptive error control strategy for grids of arbitrary topology. *Journal of Computational Physics* 1997; **138**:766–787.
7. Soria A, Ruel F. *Finite Volume Analysis of MultiComponent Incompressible Viscous Flows* (i.94.41 edn). Joint Research Centre, September 1994.
8. Diaz AR, Kikuchi N, Taylor JE. A method for grid optimization for the finite element method. *Computational Methods in Applied Mechanics and Engineering* 1983; **41**:29–45.
9. Babuska I, Zienkiewicz OC, Gago J, de A Oliverira ER. *Accuracy Estimates and Adaptive Refinements in Finite Element Computations*. Wiley: New York, 1986.
10. Mavriplis C. A posteriori error estimators for adaptive spectral element techniques. *Proceedings of the 8th GAMM Conference on Numerical Methods in Fluid Mechanics* 1990; **29**:333–342.
11. Zienkiewicz OC, Zhu JZ. A simple error estimator and adaptive procedure for practical engineering analysis. *International Journal for Numerical Methods in Engineering* 1987; **24**:337–357.
12. Smagorinsky J. General circulation experiments with the primitive equations. *Monthly Weather Review* 1963; **91**:99–152.
13. Chorin AJ. Numerical solution of the Navier–Stokes equations. *Mathematics of Computation* 1968; **23**:341–353.
14. Hirsch C. *Numerical Computation of Internal and External Flows* vol. 1. Wiley: New York, 1988.
15. Ferziger JH. Large Eddy simulation. In *Simulation and Modeling of Turbulent Flows*, Gatski TB, Hussaini MY, Lumley JL (eds), Chapter 3. Oxford University Press: Oxford, 1996, 109–154
16. Vreman B, Geurts B, Kuerten H. Comparison of numerical schemes in large Eddy simulation of the temporal mixing layer. *International Journal for Numerical Methods in Fluids* 1996; **22**:297–311.
17. Lund TS, Kaltenbach HJ, Akselvoll K. On the behaviour of centered finite difference schemes for large Eddy simulation. *Proceedings of the 6th International Symposium on Computational Fluid Dynamics*. Lake Tahoe, September 1995.
18. Cantwell B, Coles D. An experimental study of entrainment and transport in the turbulent near wake of a circular cylinder. *Journal of Fluid Mechanics* 1983; **136**:321–374.
19. Richardson LF. Atmospheric diffusion shown on a distance-neighbor graph. *Proceedings of the Royal Society of London Series* 1926; **15**:24–29.

